

# On characterization of separation force for resin replenishment enhancement in 3D printing



Dmitry Gritsenko, Alireza Ahmadian Yazdi, Yang Lin, Vladimir Hovorka, Yayue Pan, Jie Xu\*

Department of Mechanical and Industrial Engineering, University of Illinois, Chicago, IL 60607, USA

## ARTICLE INFO

### Article history:

Received 22 March 2017  
Received in revised form 9 August 2017  
Accepted 22 August 2017  
Available online 30 August 2017

### Keywords:

Separation force  
Newtonian liquid  
Constrained surface based  
stereolithography  
Surface texturing

## ABSTRACT

Additive manufacturing (AM), which is also referred to as 3D printing, is a class of manufacturing techniques that fabricate three dimensional (3D) objects by accumulating materials. Constrained surface based stereolithography is one of the most widely used AM techniques. In the process, a thin layer of liquid photosensitive resin is constrained between a constrained surface and the platform or part. The light penetrates the transparent constrained surface and cures that layer of liquid polymer. Then the platform is moved up to separate the newly cured layer to let new liquid resin fill into the gap and get cured. The separation of newly cured layer from the constrained surface is a grand challenge that limits the printable size and printing speed in this manufacturing technique. Numerous experimental works have been performed to understand how to reduce the separation force in the process. In this paper we study a new design of constrained surface with radial groove texture that significantly influences the effectiveness of reduction of the separation force and hence the manufacturing capability via theoretical modeling. In particular, we investigate the influence of groove shape, groove depth and the number of grooves on the separation force. The proposed model is validated with numerical simulations demonstrating an excellent agreement. We demonstrate the possibility of drastic reduction of the separation force (up to 112%) via surface texturing of the permeable window for continuous 3D printing.

© 2017 Elsevier B.V. All rights reserved.

## 1. Introduction

Additive manufacturing (AM), which is also referred to as 3D printing, has developed dramatically in the past decade and provided multiple commercial solutions for both industrial and public applications as summarized in literature [1,2]. AM is a class of manufacturing techniques that fabricate three dimensional (3D) objects directly from a computer-aided design (CAD) model by accumulating materials, usually in a layer by layer way. Among the various AM techniques, stereolithography (SL), also known as vat photopolymerization based AM, is one of the most widely used AM techniques currently available to the public and also the first commercialized AM technology. In SL process, a thin layer of liquid photosensitive resin is cured by an irradiation light source, such as a digital light processing (DLP) projector or a laser beam, which supplies a sufficient amount of energy to induce a curing reaction, forming highly cross-linked polymer. SL has been widely

used for applications in the fields of medical components such as hearing-aid customization and teeth model fabrication, aerospace and auto industry for rapid tooling and rapid prototyping, as well as consumer industry such as jewelry customization. SL can be classified into two types of configuration: free surface configuration in which a 3D model is fabricated by curing liquid resin which has a free surface; and constrained surface configuration in which a 3D model is fabricated by curing liquid resin constrained between the part or platform and a solid surface. Nowadays, the constrained surface based SL is more popular and most of the commercial SL machines are based on the constrained surface configuration due to advantages including faster build speed, capability of forming ultra-thin layers, and no need for containing a large vat of liquid resin for building large objects. However, despite the advances of constrained surface SL, separation of the newly cured layer from the constrained surface to allow for successful material accumulation still remains a historical challenge that limits the use and robustness of this technique [3–5]. To overcome this challenge, numerous efforts have been made by researchers in the past years. Methods such as polydimethylsiloxane (PDMS) or Teflon coating, two-way movement, tilting separation, constrained

\* Corresponding author.

E-mail address: [jjexu@uic.edu](mailto:jjexu@uic.edu) (J. Xu)

surface modification, and so on, have been developed for reducing the separation force [4–8]. In addition, experimental work has been conducted for understanding and modeling the separation force for various geometries and process conditions during the 3D printing process [8–11]. However, few research has been done for theoretical modeling and predicting the separation force.

To fill this research gap, in this paper, we develop a theoretical model for simulating and predicting the separation force under various constrained surface conditions and manufacturing process settings. As shown in Fig. 1(a), the separation force happens during the process of newly cured layer moving and new liquid filling. The constrained surface used in SL systems usually has a certain oxygen permeation capability. The oxygen permeated through the constrained surface inhibits the photopolymerization of the liquid resin near the constrained surface, thus maintaining a thin layer of liquid resin during the curing and separation process. The thickness of such layer depends on the oxygen permeability of the constrained surface and the photo-sensitivity of the liquid resin. Typically, it is  $\sim 2.5 \mu\text{m}$  thick for the conventional PDMS constrained surface and acrylic resin in SL systems. For some special highly oxygen permeable constrained surfaces, such as Teflon AF 240 and modified PDMS surface, an oxygen inhibition liquid layer with a thickness of 20–100  $\mu\text{m}$  can be obtained. Therefore, as illustrated in Fig. 1(a), after curing, a small inhibition layer near the constrained surface maintains liquid phase, and the cured part is moved up by the Z stage. The cured part needs to overcome a separation force in order to let new liquid resin fill into the gap for the curing of next layer. The separation force varied with the size and geometry of the cured layer, the liquid resin properties, the inhibition layer thickness, the constrained surface properties, and the separation speed.

In our previous work [12], a modified constrained surface, as illustrated in Fig. 1b, was developed and tested experimentally for reducing the separation force. The modified constrained surface is textured with radial grooves, as illustrated in Fig. 1(b). Experimental results showed that the radial groove constrained surface texture allows faster liquid filling and is capable of reducing separation force without losing the quality of the printed part, hence improving the printable size and the printing speed [8]. Therefore, in this paper, we focus on investigating how the radial groove surface texture affects the separation force through theoretical modeling and numerical simulations. We first obtain an analytical solution for flat window and further develop a theoretical model for a textured window based on it. The proposed model is validated with numerical simulations and demonstrates versatility with respect to varying groove depth, number of grooves and groove geometry.

## 2. Problem formulation

### 2.1. Problem definition

The governing equations describing the fluid flow within the physical domain given in Fig. 2(a), are continuity equation, coupled to the momentum equations for a transient incompressible flow of a Newtonian liquid, which is given as follows:

$$\rho \frac{D\mathbf{u}}{Dt} = -\nabla p + \nabla \cdot \boldsymbol{\tau}, \quad (1)$$

where  $\mathbf{u}$ ,  $p$ , are the velocity field and static pressure, respectively and  $\boldsymbol{\tau}$  is a stress tensor given by:

$$\boldsymbol{\tau} = \mu [\nabla \mathbf{u} + \nabla \mathbf{u}^T] \quad (2)$$

The governing equations are subjected to no-slip boundary conditions at the walls and constant atmospheric pressure at the inlet. In addition, the bottom surface of the domain is supposed to be rigid

and gravity is neglected. The separation force is derived via the integration of the static pressure over the domain top boundary  $\Omega$ :

$$F_s = \int_{\Omega} p d\Omega \quad (3)$$

### 2.2. Flat window

Introduce a cylindrical coordinate system  $(r, \theta, z)$  and consider the building of axisymmetric cylindrical part of radius  $R$ . The simplified version of Navier–Stokes equation for the radial component of velocity  $u_r$  is given by (assuming  $r \gg z$ ):

$$\frac{\partial u_r}{\partial t} = -\frac{1}{\rho} \frac{dp}{dr} + \nu \frac{\partial^2 u_r}{\partial z^2}, \quad (4)$$

with the boundary and initial conditions:

$$u_r(r, 0, t) = 0, \quad u_r(r, h, t) = 0, \quad u_r(r, z, 0) = 0, \quad (5)$$

where  $\rho$  and  $\nu$  are the density and kinematic viscosity of the resin, respectively and  $h$  is the distance between the constrained surface and the bottom surface of the cured part (further referred to as “gap”). We seek the solution of (4) and (5) in the form  $u_r(r, z, t) = -u(r, z, t) + f(r, z)$  that allows to present a non-homogeneous (4) as a homogeneous system:

$$\frac{\partial u}{\partial t} = \nu \frac{\partial^2 u}{\partial z^2} \quad (6)$$

$$\frac{1}{\rho} \frac{dp}{dr} = \nu \frac{\partial^2 f(r, z)}{\partial z^2} \quad (7)$$

with boundary conditions for  $f(r, z)$ :

$$f(r, 0) = 0, \quad f(r, h) = 0. \quad (8)$$

Solving (6), (7) with (5) and (8) we obtain  $u_r(r, z, t)$ :

$$u_r(r, z, t) = \frac{2h^2}{\mu} \frac{dp}{dr} \sum_{n=1}^{\infty} \frac{(-1)^n - 1}{\pi^3 n^3} \sin\left(\frac{\pi n z}{h}\right) e^{-\left(\frac{\pi n}{h}\right)^2 \nu t} + \frac{h^2}{2\mu} \frac{dp}{dr} \left\{ \left(\frac{z}{h}\right)^2 - \frac{z}{h} \right\}, \quad (9)$$

where  $\mu = \nu\rho$  is the dynamic viscosity of the resin. Applying mass conservation to the considered physical domain (cylinder) we arrive at:

$$\frac{dV}{dt} = 2\pi r \int_0^h u_r(r, z, t) dz, \quad (10)$$

where  $V = \pi r^2 h$  is the volume of the cylinder. Thus we get:

$$\frac{dh}{dt} = \frac{4h^3}{\mu} \frac{dp}{dr} \sum_{n=1}^{\infty} \frac{\{(-1)^n - 1\}^2}{\pi^4 n^4} e^{-\left(\frac{\pi n}{h}\right)^2 \nu t} + \frac{h^3}{6\mu} \frac{dp}{dr} \quad (11)$$

Let us further assume that the part elevation changes with a constant speed  $V_0$ , i.e.  $h = h_0 + V_0 t$ . Then (11) can be reduced to:

$$V_0 = \frac{\beta}{r} \frac{dp}{dr} h^3 (\alpha + 1), \quad (12)$$

where  $\beta = 1/6\mu$  and  $\alpha = 24 \sum_{n=1}^{\infty} \frac{\{(-1)^n - 1\}^2}{\pi^4 n^4} e^{-\left(\frac{\pi n}{h}\right)^2 \nu t}$ . Subsequent integration through the entire domain allows the separation pressure and separation force to be formed:

$$p_s = -\frac{V_0}{2h^3 \beta (\alpha + 1)} (r^2 - R^2), \quad F_s = \frac{V_0 \pi R^4}{4\beta h^3 (1 + \alpha)} \quad (13)$$

The maximum value of the separation force can be obtained via solving the two-parameter optimization problem with respect to  $V_0$  and  $t$  and achieved at  $h_0 = 2V_0 t$ .

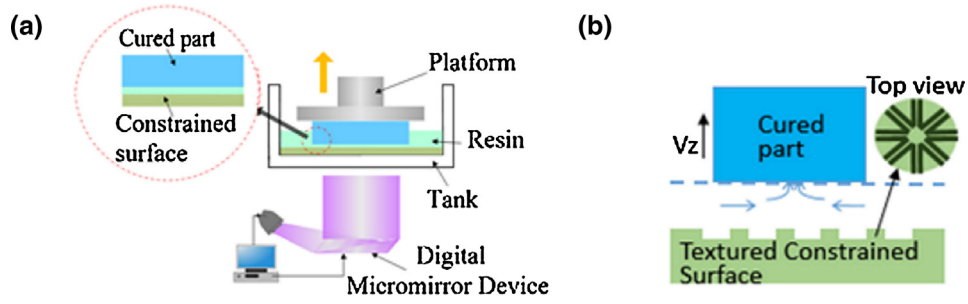


Fig. 1. Continuous 3D printing operating principle: (a) schematic of constrained surface based stereolithography system and (b) illustration of textured constrained surface.

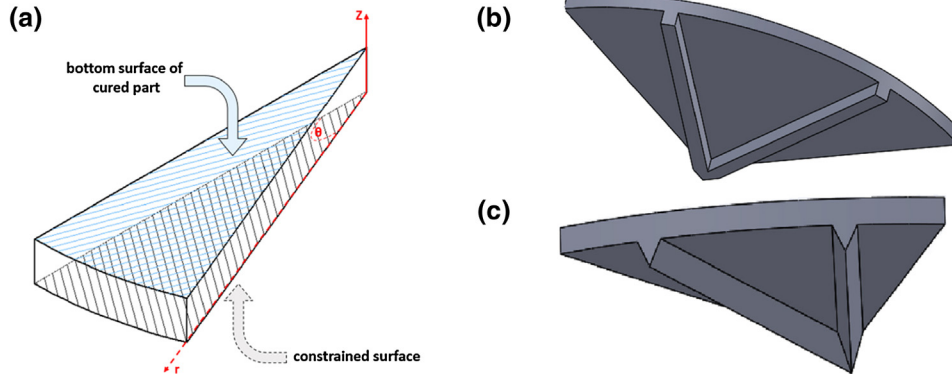


Fig. 2. Fluid simulation domain (a) schematic with reference frame (b) a patterned window with rectangular grooves ( $n = 16$ ,  $h_{gr} = 1$  mm) and (c) a patterned window with triangular grooves ( $n = 16$ ,  $h_{gr} = 1$  mm).

### 2.3. Patterned window

Consider the window surface patterned with radially symmetric grooves. It is expected that these grooves will enhance the flow by increasing the cross section of flow pathway. Thus we propose a model for the estimation of the separation force for the window patterned with radial grooves based on the analytical solution for a flat window. Introduce the concept of the effective gap:

$$h_{eff} = h_0 + \left( \frac{S_{gr}}{S_{gap}} \right)^{\gamma_{ij}} h_{gr}, \quad (14)$$

where  $h_0$  is the initial gap for the flat window,  $S_{gr}$  is the total area of the bottom surfaces of the grooves,  $S_{gap}$  is the total area of the flat window and  $\gamma_{ij}$  is a fitting function dependent on the geometry of the grooves. The concept is based on mass conservation of the liquid domain formed by the patterned window and the equivalent flat window with increased gap due to the presence of grooves. We studied three cases: (1) varying the number of grooves with fixed groove depth ( $h_{gr} = 1$  mm) and fixed groove geometry (rectangular) (2) varying groove depth with a fixed number of grooves ( $n = 16$ ) and fixed groove geometry (rectangular) (3) varying groove depth and varying groove geometry (rectangular and triangular) with a fixed number of grooves ( $n = 16$ ).

#### 2.3.1. Varying groove depth

The number of grooves was chosen to be  $n = 16$  while the groove depth was varied from 0 to 4 mm by 0.5 mm steps. We seek  $\gamma_{ij}$  as a third order polynomial:

$$\gamma_{ij} = 1 + \varepsilon_i \delta_j + \frac{1}{2!} (\varepsilon_i \delta_j)^2 + \frac{1}{3!} (\varepsilon_i \delta_j)^3, \quad (15)$$

where  $\delta_j$  is a fitting function derived below and  $\varepsilon_i = F_1/F_i$  with  $F_1$  to be the maximum value of the separation force for a flat window with 1 mm gap derived from (13) and  $F_i$  to be the maximum value

of the separation force for the patterned window obtained from the simulation. However, the dependence of  $\gamma_{ij}$  on the groove depth  $h_{gr}$  has not been implemented yet. When seeking its explicit form we assume that (1)  $\delta_j(0) = 0$ ; (2)  $\delta_j$  is finite,  $|\delta_j| \leq M$ , where  $M$  is a finite number; (3)  $\delta_j$  reaches saturation as  $h_{gr} \rightarrow h_{\infty}$ . We assume  $h_{\infty} = R$ . Thus the explicit form of  $\delta_{1,3}$  is:

$$\delta_{1,3}(h_{gr}) = \phi_{1,3} (1 - e^{-\psi_{1,3}(h_{gr}/h_{\infty})}), \quad (16)$$

where  $\phi_{1,3}$  and  $\psi_{1,3}$  are fitting parameters and the subscripts “1, 3” correspond to the cases of rectangular and triangular grooves, respectively. With  $\delta_{1,3}$  given we now seek an explicit dependence of the maximum separation force from the grooves depth. It decays exponentially according to:

$$F_{\max,1}(h_{gr}) = \xi_1 e^{-0.5(h_{gr}/h_{\infty})^{1/3}} \quad (17)$$

$$F_{\max,3}(h_{gr}) = \xi_3 e^{-(h_{gr}/h_{\infty})^{1/3}}, \quad (18)$$

where  $\xi_1$  and  $\xi_3$  are fitting parameters. System (13)–(18) forms a complete set of equations to describe the maximal separation force for the patterned window with respect to groove depth.

#### 2.3.2. Varying number of grooves

We now seek  $\delta_j$  for the case of the fixed groove depth ( $h_{gr} = 1$  mm) and changing the number of grooves ( $n = 8, \dots, 72$  with the step  $\Delta n = 8$ ). We again use (15) for fitting of  $\gamma_{ij}$  first. We further intend to find the dependence of  $h_{eff}$  from the number of grooves  $n$ . To do so, we introduce  $\delta_2(n)$  as follows:

$$\delta_2(n) = 1 - e^{-\psi_2(n/n_{\infty})}, \quad (19)$$

where  $n_{\infty} = 128$ , that corresponds to complete coverage of the window with grooves and the subscript “2” corresponds to the case of the rectangular grooves. With  $\delta_2$  given, we now seek an explicit

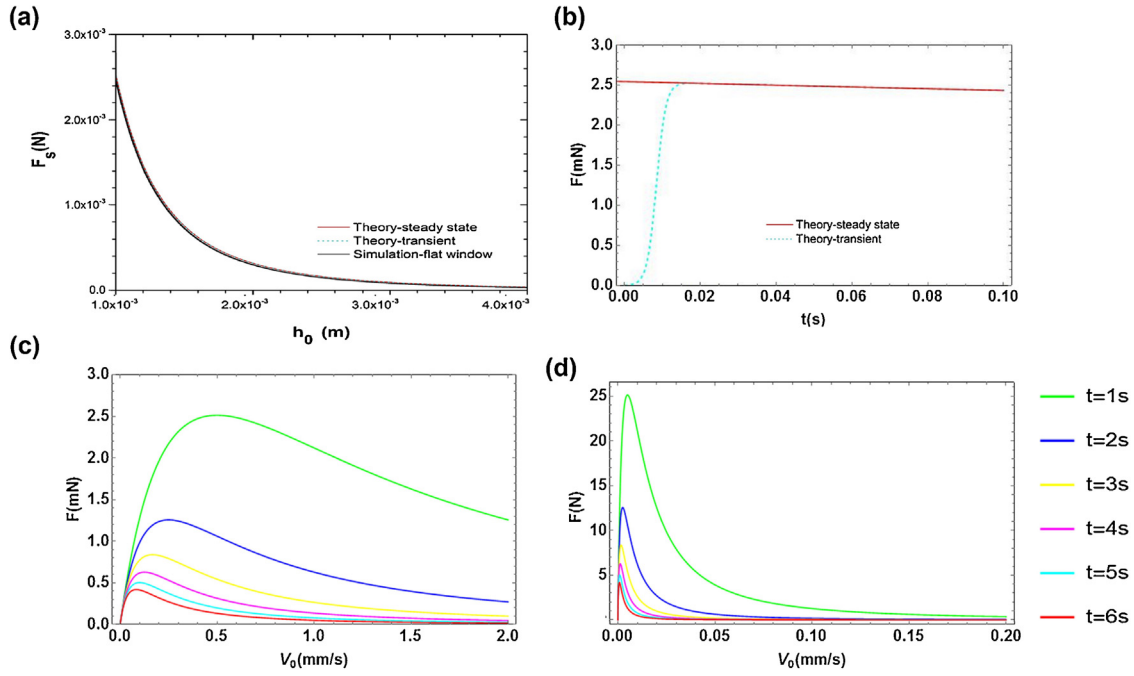


**Fig. 3.** Separation force dependence from (a) the gap for the flat window with 1 mm initial gap: solid black line represents simulation results, dashed cyan and solid red lines represent steady state and transient theoretical solutions, respectively (b) the difference between steady state and transient solutions for small times ( $t < 0.1$  s) (c) elevation speed with  $h_0 = 1$  mm (d) elevation speed with  $h_0 = 10 \mu\text{m}$ . The legend “t” in (c) and (d) corresponds to the different moments of time. (For interpretation of the references to color in this legend, the reader is referred to the web version of the article.)

dependence of the maximum separation force on the number of grooves. It decays exponentially according to:

$$F_{\max,2}(n) = \xi_2 e^{-\zeta_2(n/n_\infty)} \quad (20)$$

System (13)–(15), (19) and (20) forms a complete set of equations to describe the maximum suction force for a patterned window with respect to the number of grooves.

### 3. Methods

Governing Eqs. (1)–(3) were solved numerically in commercial software (ANSYS Fluent 16.2) using finite volume method in the domain of interest (segment of the disc, flat and patterned, with radius  $R = 20$  mm, height  $h_0 = 1$  mm). The sample geometries of the patterned fluid domains are given at Fig. 2(b) and (c).

The simulation were shown to be mesh-independent for the entire volume mesh elements number ranging from  $2 \times 10^5$  to  $8 \times 10^5$ . The resin flow was considered as laminar, with resin density  $\rho = 1100 \text{ kg/m}^3$  and viscosity  $\mu = 0.09 \text{ kg/(m s)}$ . The elevation speed was set at  $V_0 = 0.15 \text{ mm/s}$  and controlled by a user-defined function (UDF) given at customized C script. Finally, gravity was neglected. Theoretical modeling and statistical data analysis were done with Wolfram Mathematica 11 using customized scripts. For each fitting an array of  $\sim 3 \times 10^4$  data points was used.

## 4. Results and discussion

### 4.1. Flat window

The expression for  $F_s$  in (13) was first used to fit the numerical simulations results for the flat window with 1 mm initial gap. It showed an excellent agreement with the theoretical predictions (Fig. 3(a)).

The crucial difference between steady-state and transient solutions is shown in Fig. 3(b). The transient solution allows to satisfy initial condition for the separation force  $F(0) = 0$ . The separation force also demonstrates resonant behavior as a function of ele-

**Table 1**  
Fitting parameters statistics.

Parameter	Value	Error	t-Statistic	p-Value
$\psi_1$	0.50	$9.66 \times 10^{-3}$	51.49	$2.73 \times 10^{-10}$
$\phi_1$	89.75	9.02	9.95	$2.21 \times 10^{-5}$
$\xi_1$	1.07	$4.97 \times 10^{-3}$	214.18	$2.53 \times 10^{-16}$
$\psi_2$	4.35	0.31	14.12	$6.15 \times 10^{-7}$
$\xi_2$	2.42	$2.25 \times 10^{-2}$	107.85	$1.55 \times 10^{-12}$
$\zeta_2$	1.25	$3.17 \times 10^{-2}$	39.61	$1.70 \times 10^{-9}$
$\phi_3$	27.49	2.05	13.42	$1.06 \times 10^{-5}$
$\psi_3$	0.48	$8.51 \times 10^{-3}$	56.34	$2.10 \times 10^{-9}$
$\xi_3$	1.01	$1.19 \times 10^{-3}$	846.46	$8.48 \times 10^{-19}$

vation speed (Fig. 3(c)). Moreover, the local maximums of the separation force for a flat window with 1 mm gap are achieved for the elevation speeds close enough to the one chosen for simulations. Thus, the “worst case” is considered allowing even stronger reduction of the separation force when shifting far away from the resonance. Fig. 3(d) shows the separation force dependence from the elevation speed for reduced gap size ( $h_0 = 10 \mu\text{m}$ ). It demonstrates the similar resonant behavior with the resonant peak shifted to lower elevation speeds.

### 4.2. Patterned window

The simulation results for the parameters  $\delta_{1,3}(h_{gr})$  were fitted with (16) as shown in Fig. 4(a). It demonstrates an excellent agreement between theoretical model and simulation results (Table 1). Finally, the maximal separation force was fitted with (18). Fig. 5(a) compares the results of theoretical modeling and numerical simulations for maximal separation force as a function of groove depth  $h_{gr}$ . It indicates an excellent agreement between the proposed model and numerical simulations (Table 1).

To fit the parameter  $\delta_2(n)$  Eq. (19) was used. The fitting results are given at Fig. 4(b) and show excellent agreement between the simulation results and theory (Table 1). In particular,  $\delta_2 = 0$  as  $n \rightarrow 0$  and  $\delta_2 \rightarrow 1$  as  $n \rightarrow n_\infty$ . Fig. 5(b) compares the results of theoret-

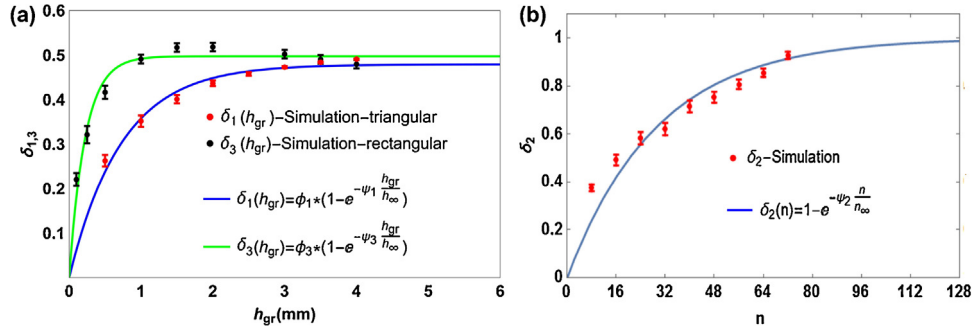


Fig. 4. The dependence of the fitting parameter  $s\delta_j$  ( $j = 1, 2, 3$ ) from (a) the groove depth for rectangular and triangular grooves. Dots represent simulation results, solid lines represent fitting results (b) the number of grooves. Dots represent simulation results, solid lines represent fitting results.

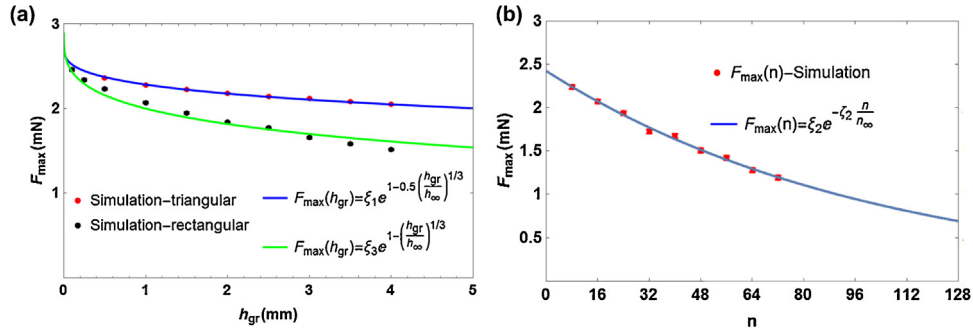


Fig. 5. The dependence of maximal separation force from (a) the groove depth for rectangular and triangular grooves. Dots represent simulation results, solid lines represent fitting results (b) the number of grooves. Dots represent simulation results, solid lines represent fitting results.

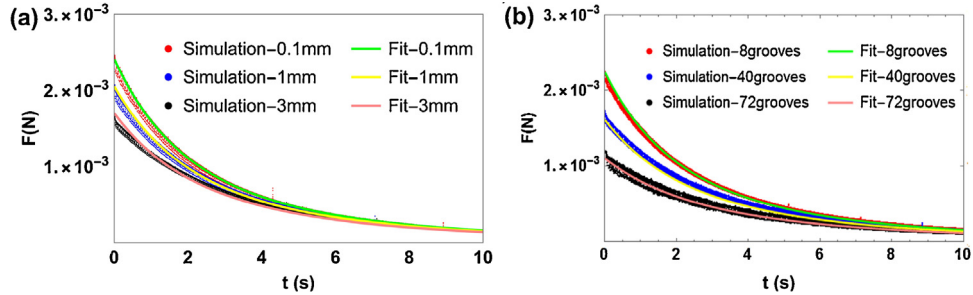


Fig. 6. Time dependence of the separation force for (a) fixed number of grooves ( $n = 16$ ) and varying groove depth. The groove depth ranges from 0.5 to 4 mm with 0.5 mm step (b) fixed groove depth ( $h_{gr} = 1$  mm) and varying number of grooves. The number of grooves ranges from 8 to 72 with  $\Delta n = 8$  step. Dotted lines represent simulation results, solid lines represent fitting results.

cal modeling and numerical simulations for maximum separation force as a function of the number of grooves  $n$ .

It indicates an excellent agreement between the proposed model (20) and numerical simulations (Table 1).

Finally, we can apply the models (13)–(18), (13)–(15), (19) and (20) to fit the simulation data. The fitting results for the separation force time dependence with varying groove depth are given in Fig. 6(a) and show excellent agreement (Table 1). The reduction of maximal separation force up to 67% with respect to the flat window with a 1 mm gap was achieved.

The comparison of the theoretical modeling and simulation results for the separation force time dependence with varying groove number is given in Fig. 6(b). The reduction of the maximal separation force can be defined as:

$$\chi = 1 - \frac{F_{s,flat}|_{h_0=2V_0t}}{F_{s,patterned}|_{h_0=2V_0t}}, \quad (21)$$

where  $F_{s,flat}$  and  $F_{s,patterned}$  correspond to the separation for the flat and patterned windows, respectively. The difference between them is that for the latter  $h_0$  was replaced with  $h_{eff}$  according to (14). The reduction of the maximal separation force up to 112% with respect to the flat window with a 1 mm gap was demonstrated. Fig. 6(a) and (b) confirms the effectiveness of the patterned window in speeding up the resin replenishment.

After the implementation of the concept of the effective gap an expression for the separation force becomes:

$$F_s = \frac{V_0 \pi R^4}{4\beta \left( h_0 + \left( \frac{S_{gr}}{S_{gap}} \right)^{\gamma_{ij}} h_{gr} + V_0 t \right)^3 \left( 1 + 24 \sum_{n=1}^{\infty} \frac{\{(-1)^n - 1\}^2}{\pi^4 n^4} e^{-\left( (\pi n) / \left( h_0 + \left( \frac{S_{gr}}{S_{gap}} \right)^{\gamma_{ij}} h_{gr} + V_0 t \right) \right)^2 vt} \right)} \quad (22)$$

#### 4.3. Groove shape effect

We also considered the influence of the groove shape on the separation force. The comparison of the fitting parameter  $\delta_j$  dependence on the groove depth for rectangular and triangular grooves is given at Fig. 4(a). It clearly shows that the saturation values are close for both geometries  $\delta_{1,3,sat} \rightarrow 0.5$  and the saturation of the  $\delta_j$  is achieved faster for the rectangular grooves. Moreover, when using triangular grooves the reduction of the maximal separation force is not significant compared to rectangular grooves and reaches up to 23% only. This result can be explained as follows. The volume of the triangular grooves is less than the volume of the rectangular ones. Consequently,  $h_{eff}$  is less for triangular grooves, that in turn leads to a smaller reduction of the maximum separation force.

#### 5. Conclusion

We developed a theoretical model for the prediction of the separation force for a patterned window and demonstrated the possibility of significant reduction (up to 112%) of the separation force for continuous 3D printing. Two parameters, groove depth and the number of grooves, were taken into account. If optimized simultaneously an even better reduction of the separation force can be achieved.

#### Acknowledgements

This research was supported by National Science Foundation (Grant 1563477).

#### References

- [1] A.A. Yazdi, A. Popma, W. Wong, T. Nguyen, Y. Pan, J. Xu, 3D printing: an emerging tool for novel microfluidics and lab-on-a-chip applications, *Microfluid. Nanofluidics* 20 (3) (2016) 1–18.
- [2] J.W. Stansbury, M.J. Idacavage, 3D printing with polymers: challenges among expanding options and opportunities, *Dent. Mater. J.* 32 (1) (2016) 54–64.
- [3] K. Ikuta, K. Hirawatari, Real three dimensional micro fabrication using stereo lithography and metal molding, in: *Micro Electro Mechanical Systems, 1993, MEMS'93, IEEE Proceedings: An Investigation of Micro Structures, Sensors, Actuators, Machines and Systems, IEEE, 1993*, pp. 42–47.
- [4] Y. Pan, C. Zhou, Y. Chen, A fast mask projection stereolithography process for fabricating digital models in minutes, *J. Manuf. Sci. Eng.* 134 (5) (2012) 051011.
- [5] P.M. Lambert, E.A. Campaigne III, C.B. Williams, Design considerations for mask projection microstereolithography systems, in: *Proceedings of the Solid Freeform Fabrication Symposium*, vol. 111, 2013.
- [6] H. John, Apparatus and method for the non-destructive separation of hardened material layers from a at construction plane, US Patent 7,438,846, 2008.
- [7] C. Zhou, Y. Chen, Z. Yang, B. Khoshnevis, Development of multimaterial mask-image-projection-based stereolithography for the fabrication of digital materials, in: *Annual Solid Freeform Fabrication Symposium, Austin, TX, 2011*.
- [8] H. He, Y. Pan, J. Xu, X. Yu, V. Botton, Fast mask image projection-based micro-stereolithography process for complex geometry, in: *11th International Conference on Micro Manufacturing, ICOMM 2016, Irvine, California, March 29–31, 2016*.
- [9] Y.-M. Huang, C.-P. Jiang, On-line force monitoring of platform ascending rapid prototyping system, *J. Mater. Process. Technol.* 159 (2) (2005) 257–264.
- [10] Y. Pan, H. He, J. Xu, A. Feinerman, Study of separation force in constrained surface projection stereolithography, *Rapid Prototyp. J.* 23 (2) (2017).
- [11] Y. Pan, Y. Chen, Z. Yu, Fast mask image projection-based micro-stereolithography process for complex geometry, *J. Micro Nano-Manuf.* 5 (1) (2017) 014501.
- [12] Y. Pan, Y. Chen, Z. Yu, Effect of surface texturing on separation force in projection stereolithography, *J. Micro Nano-Manuf.* 5 (1) (2017) 014501.